Title
Reelin Deficiency Delays Mammary Tumor Growth and Metastatic Progression

Journal
Journal of Mammary Gland Biology and Neoplasia, 22(1)

ISSN
1083-3021

Authors
Khialeeva, Elvira
Chou, Joan W
Allen, Denise E
et al.

Publication Date
2017-03-01

DOI
10.1007/s10911-017-9373-z

Peer reviewed

Published in final edited form as:

J Mammary Gland Biol Neoplasia. 2017 March ; 22(1): 59–69. doi:10.1007/s10911-017-9373-z.

Reelin Deficiency Delays Mammary Tumor Growth and Metastatic Progression

Elvira Khialeeva[1], **Joan W. Chou**[2], **Denise E. Allen**[3], **Alec M. Chiu**[4], **Steven J. Bensinger**[5,6,7], and **Ellen M. Carpenter**[1,8]

[1]Molecular Biology Institute, University of California Los Angeles, Los Angeles, CA, United States of America. ekhiale@ucla.edu

[2]Department of Integrative Biology and Physiology, University of California Los Angeles, Los Angeles, CA, United States of America. chou.joan1919@gmail.com

[3]Department of Molecular, Cell, and Developmental Biology, University of California Los Angeles, Los Angeles, United States of America. denalle@ucla.edu

[4]Department of Chemistry and Biochemistry, University of California Los Angeles, Los Angeles, United States of America. alecmchiu@ucla.edu

[5]Department of Molecular and Medical Pharmacology, University of California Los Angeles, Los Angeles, United States of America. sbensinger@mednet.ucla.edu

[6]Department of Microbiology, Immunology, and Molecular Genetics, University of California Los Angeles, Los Angeles, United States of America

[7]Department of Pathology and Laboratory Medicine, University of California Los Angeles, Los Angeles, United States of America

[8]Department of Psychiatry and Biobehavioral Sciences, University of California Los Angeles, Los Angeles, United States of America. ecarpenter@mednet.ucla.edu

Abstract

Reelin is a regulator of cell migration in the nervous system, and has other functions in the development of a number of non-neuronal tissues. In addition, alterations in reelin expression levels have been reported in breast, pancreatic, liver, gastric, and other cancers. Reelin is normally expressed in mammary gland stromal cells, but whether stromal reelin contributes to breast cancer progression is unknown. Herein, we used a syngeneic mouse mammary tumor transplantation model to examine the impact of host-derived reelin on breast cancer progression. We found that transplanted syngeneic tumors grew more slowly in reelin-deficient ($rl^{Orl\ -/-}$) mice and had delayed metastatic colonization of the lungs. Immunohistochemistry of primary tumors revealed

Correspondence to: Elvira Khialeeva.

Conflict of Interest

The authors declare that they have no conflict of interest.

Compliance with Ethical Standards

Ethics approval

All animal studies were conducted in accordance with the UCLA Office of Animal Research Oversight and Institutional Animal Care and Use Committee protocols.

that tumors grown in $rl^{Orl\ -/-}$ animals had fewer blood vessels and increased macrophage infiltration. Gene expression studies from tumor tissues indicate that loss of host derived reelin alters the balance of M1- and M2-associated macrophage markers, suggesting that reelin may influence the polarization of these cells. Consistent with this, $rl^{Orl\ -/-}$ M1-polarized bone marrow-derived macrophages have heightened levels of the M1-associated cytokines *iNOS* and *IL-6*. Based on these observations, we propose a novel function for the reelin protein in breast cancer progression.

Keywords

Reelin; breast cancer; 4T1; tumor-associated macrophage

Introduction

The reelin signaling pathway is widely recognized as an important regulator of cell migration in the developing central nervous system [1–4]. Reelin is a glycoprotein secreted into the extracellular matrix, and canonically signals by binding to low-density lipoprotein receptors Apo E receptor 2 (ApoER2) and very low-density lipoprotein receptor (VLDLR) located on the surface of reelin-responsive cells [5]. Binding of reelin to its receptors recruits the intracellular adaptor protein Disabled-1 (Dab1), which is phosphorylated by Src family kinases on tyrosine residues [6,7]. Phosphorylated Dab1 activates multiple downstream effectors, including phosphatidylinositol-3-kinase (PI3K)/Akt and C3G/Rap1 [2]. This cascade of signaling events leads to changes in cytoskeleton stabilization, allowing reelin to orchestrate cell migration in the central nervous system.

Recent studies have identified a number of non-neuronal functions for reelin [8–12]. For example, reelin signaling was found to regulate the homeostasis of the intestinal crypt-villus unit [11], formation of thrombin clots [10], and to be important for establishment of the lymphatic vasculature [12]. Our laboratory found that canonical reelin signaling is essential for proper mammary gland development [13]. Reelin is normally expressed in the myoepithelial layer and the stroma of the developing and mature mammary ducts, while Dab1 is expressed in the luminal epithelium. Reelin and Dab1 coordinate ductal extension and refine the morphology of the mammary ducts. Absence of functional reelin signaling results in ductal growth delays, abnormal branching patterns and disorganized cellular layers within the mammary ducts [13]. Alterations in reelin signaling have been reported in pancreatic, gastric, prostate, and esophageal cancers [14–17]. Interestingly, reelin expression is lost in many human breast tumors, and the loss of reelin protein correlates with poor survival [18], but the mechanisms by which reelin may affect breast cancer progression *in vivo* remain to be determined.

To better understand the relationship between reelin signaling and breast cancer, we monitored mammary tumor growth and metastatic progression following transplantation of 4T1 mouse mammary tumor cells into mice that lack functional reelin protein ($rl^{Orl\ -/-}$). We chose the 4T1 mammary tumor transplantation model for two reasons. First, 4T1 cells mimic stage IV human breast cancer, and rapidly form primary tumors and spontaneous lung

metastases when orthotopically injected into Balb/C mice [19]. Second, the 4T1 model allows us to study tumor progression in immunocompetent mice carrying the *rl*^{Orl} mutation, and provides us with the ability to address the contribution of the host immune response to the growth of primary tumors and metastasis.

We report that the absence of reelin from the host environment delays primary tumor growth and metastatic spread of mammary carcinoma cells, possibly via alterations in the cytokine expression profile of tumor-associated macrophages (TAMs). Loss of reelin does not directly affect proliferation or migration of tumor cells, but may modulate the activation of macrophages in the tumor microenvironment, diminishing their tumor-promoting properties. Our results indicate a novel function for the reelin protein in mammary tumor progression, and suggest possible roles for reelin in macrophage activation.

Materials and Methods

Mice

Balb/C mice were purchased from Charles River Laboratories. *Reeler Orleans* (*rl*$^{Orl\ -/-}$) mice were obtained from a breeding colony maintained at UCLA. These mice carry a naturally occurring mutation, in which a transposon insertion leads to exon skipping and a 220 bp deletion in the *reelin* mRNA [20]. The resulting reelin protein is truncated and is not secreted [21]. *Rl*^{Orl} mice were initially on a mixed, 70–75% Balb/C and 20–25% 129/Sv background, and were backcrossed to the Balb/C strain for three generations to obtain ≥95% Balb/C offspring. The genetic background of the *rl*^{Orl} line was confirmed by single nucleotide polymorphism (SNP) scanning (The Jackson Laboratory). The use of a Balb/C background is necessary for histocompatibility, as 4T1 cells are derived from Balb/C mice [19]. Homozygous mutant and wild type control female offspring were obtained from intercrosses of heterozygous *rl*$^{Orl\ +/-}$ animals. *Rl*^{Orl} mice were genotyped by PCR as described [20].

Cell Lines

The 4T1 cell line was purchased from American Type Culture Collection, and maintained according to ATCC guidelines. Cells were cultured in RPMI-1640 medium (Life Technologies) supplemented with 10% fetal bovine serum (FBS, Omega) and 100 u/mL penicillin/streptomycin (Life Technologies). Sub-confluent cultures were treated with 0.25% trypsin-EDTA (Life Technologies) and passaged, or counted using a hemocytometer and used for *in vitro* or *in vivo* experiments.

The reelin-secreting HEK293T cell line (stably transfected with a full-length reelin clone) [22] was kindly provided by Dr. Tom Curran, Children's Hospital of Philadelphia, PA, USA. The control HEK293T cell line was kindly provided by Dr. Harley Kornblum, University of California Los Angeles, CA, USA. Both cell lines were cultured in DMEM (Life Technologies) supplemented with 10% FBS and 100 u/mL penicillin/streptomycin. Conditioned media was collected from confluent cells after 48 hours of culture, centrifuged at 600 g for 10 min, and the supernatant was collected and used immediately for treatment of 4T1 cells and migration assays.

Mammary Epithelial Cell (MEC) Purification

MECs were purified as previously described [23]. Briefly, pairs of #3 thoracic and #4 inguinal mammary glands were dissected from 8–10 week-old female mice, minced and incubated in DMEM/F12 (Corning) containing 5% FBS, 100 u/mL penicillin/streptomycin, 2 mg/mL collagenase IV (Sigma), 2 mg/mL trypsin (Sigma), and 5 μg/mL insulin (Life Technologies) on an orbital shaker at 100 RPM, 37°C, for 1 hr. Digested tissue was treated with 4 u/mL DNAse (Sigma), and organoids containing MECs were purified by repeated pulse centrifugation.

Transwell Migration Assay

10^5 4T1 cells in serum-free DMEM were seeded on top of Boyden transwells fitted with membranes containing 8 μm pores, and allowed to migrate overnight in response to conditioned media from reelin-secreting HEK293T cells or control HEK293T cells with 10% FBS. Cell nuclei were stained with DAPI, and membranes were imaged on a Zeiss Axioskop with a cooled CCD camera. Four evenly spaced 100X fields per membrane were photographed and used to count the number of cells that migrated through the membrane. Cell counts were used to determine the average number of migrating cells for each membrane.

Tumor Challenge

10^5 4T1 cells in HBSS were injected into the left #4 mammary fat pad of homozygous mutant and control wild type rl^{Orl} 8–10 week-old female mice. The tumor diameters were measured every 3–4 days beginning on day 11 after transplantation using electronic calipers. The tumor volume was calculated using the formula $L \times W^2 \times 0.52$, where L = longest diameter, and W = perpendicular diameter [24]. All mice were sacrificed before the primary tumor diameter reached 1.5 cm or when the animals became moribund.

Micrometastasis Assay

Lungs from tumor-bearing mutant and wild type rl^{Orl} mice were dissected in sterile conditions, and lung tissue was processed as described [19]. Briefly, lungs were minced and incubated in digestion buffer containing collagenase I (Sigma) for 1 hour at 37°C. Digested tissue was sieved through 70 μm cell strainers, and red blood cells were lysed in RBC lysis buffer (StemCell Technologies). The resulting cell suspension was serially diluted into 6-well plates in RPMI-1640 medium supplemented with FBS and penicillin/streptomycin. The next day, medium was replaced with complete RPMI-1640 containing 60 μM 6-thioguanine. After 10 days of incubation, resistant 4T1 colonies were stained with methylene blue and counted. The number of 4T1 colonies was equated to the number of 4T1 cells in the seeded cell suspension, normalized to the number of cells plated, and the resulting percentage was reported as the metastatic burden.

Immunohistochemistry and Histology

For paraffin-embedded samples, dissected tumor slices were fixed overnight in Bouin's fixative, washed, dehydrated, and embedded in paraffin. For frozen samples, tumor slices

were fixed in 4% paraformaldehyde for 4 hours, cryoprotected in 30% sucrose and embedded in Optimal Cutting Temperature compound (Sakura).

For Ki-67 and CD31 labeling, paraffin-embedded samples were sectioned at 10 μm. The sections were rehydrated through graded ethanols and boiled in 10 mM sodium citrate buffer to retrieve antigens. After blocking endogenous peroxidases, as well as avidin and biotin, sections were incubated with primary, and then biotinylated secondary antibodies. The antibodies used were rabbit anti-Ki-67 (1:500, Vector Labs), rat anti-CD31 (1:200, Dianova), biotinylated goat anti-rabbit (1:500, Jackson Immunoresearch), biotinylated donkey anti-rat (1:500, Jackson Immunoresearch). The antibodies were visualized using an ABC Elite Kit (Vector Labs) and diaminobenzidine (DAB) staining. Cell nuclei were counterstained with hematoxylin.

For F4/80 labeling, 10 μm frozen sections were treated with 1% Triton X-100 (Sigma), blocked with donkey serum, and incubated with primary antibody, then AlexaFluor 594-conjugated secondary antibody. Cell nuclei were counterstained with DAPI. The antibodies used were rat anti-F4/80 (1:1000, Abbiotec), Alexa Fluor 594 donkey anti-rat (1:500, Life Technologies).

For histological evaluation of tumor sections, 10 μm paraffin sections were rehydrated through graded ethanols and stained with hematoxylin and eosin.

For Ki-67 labeling analysis, Ki-67-positive and Ki-67-negative cell nuclei were counted in 4 random fields per sample using the ObjectJ plugin in ImageJ (NIH), and the average percentage of Ki-67-positive nuclei was calculated for each sample. Each analyzed field contained at least 500 total cells. For CD31 and F4/80 labeling analysis, 6 random 200X fields per sample were imaged, DAB signal (for CD31) or AlexaFluor 594 signal (for F4/80) was thresholded in ImageJ, and the average percentage of CD31-positive or F4/80-positive area was calculated for each sample.

Quantitative PCR (qPCR)

RNA from tumor tissues or cells was extracted using TRI reagent (Sigma), and the cDNA was generated using an iScript cDNA Synthesis kit (Bio-Rad). qPCR was carried out using the KAPA SYBR FAST master mix (KAPA Biosystems) on a Light Cycler 480 (Roche). Expression values were normalized to the housekeeping gene *36b4/RPLP0*. Primer sequences are listed in Table 1.

Western Blotting

Tumor tissue was homogenized in radioimmunoprecipitation (RIPA) buffer containing phosphatase inhibitor cocktail (Zmtech scientific). Protein samples (35 μg) were separated on 4–12% Bis-Tris SDS-PAGE gels (Life Technologies), and transferred onto Immuno-Blot PVDF membranes (Bio-Rad). Membranes were blocked in PBS with 5% skim milk and 0.1% Tween-20 for 1 hour, and incubated with primary antibodies overnight at 4°C, then with secondary antibodies for 30 min at room temperature. Protein bands were detected using the ECL Western blotting detection reagent (GE Amersham). Band intensities were quantified using ImageJ and relative protein levels were normalized to β-actin levels. The

following antibodies were used: mouse anti-arginase-1 (1:4000, BD Biosciences), mouse anti-β-actin (1:10,000, Sigma), mouse anti-reelin (1:500, Millipore), peroxidase conjugated goat anti-mouse (1:3000, Cell Signaling).

Bone Marrow-Derived Macrophage (BMDM) Culture

Femurs and tibias were collected from 6–8 week old female mutant and wild type *rl*^{Orl} mice. BMDM cultures were prepared as described [25]. Briefly, the bone marrow was flushed and passed through 26G needles to generate a single cell suspension and the red blood cells were lysed in RBC lysis buffer. The remaining cells were counted, and equal numbers were plated into 6-well plates. Macrophages were differentiated over the course of 7 days in DMEM with addition of 20% FBS, 100 u/mL penicillin/streptomycin, 2 mM L-glutamine (Life Technologies), 0.5 mM sodium pyruvate (Life Technologies), and 5% conditioned media from CMG 14-12 cells, which contains macrophage colony-stimulating factor (M-CSF). For 4T1-conditioned medium studies, medium was collected from 4T1 cells after 48 hours of culture. BMDM were treated with 4T1-conditioned medium for 24 hours. To generate M1 polarized macrophages, BMDM were treated with 50 ng/mL IFN-γ (Life Technologies) and 100 ng/mL LPS (InvivoGen) overnight.

Results

Reelin influences mammary tumor growth and metastasis *in vivo*

Loss of reelin expression in breast tumors correlates with poor patient prognosis and survival [18]. In order to better understand the impact of reelin on the progression of breast cancer, we examined growth of 4T1-derived mouse mammary tumors in syngeneic reelin-deficient mice (*rl*$^{Orl\ -/-}$). Tumor development was initiated by injecting the mammary fat pads of female *rl*$^{Orl\ -/-}$ mice or wild type *rl*$^{Orl\ +/+}$ controls with 10^5 4T1 cells. Primary tumors grew more slowly in *rl*$^{Orl\ -/-}$ mice (Fig. 1a), and weighed significantly less than tumors from *rl*$^{Orl\ +/+}$ control mice 25 days after the 4T1 cell injection (Fig. 1b). Mice with mutations in the *reelin* gene are usually smaller in size than their wild type and heterozygous littermates [26], and the *rl*$^{Orl\ -/-}$ mice used in our study also weighed significantly less than the *rl*$^{Orl\ +/+}$ controls (Fig. 1c). However, tumor growth had no impact on the overall weight of tumor-bearing animals, as the body weight of *rl*$^{Orl\ -/-}$ and *rl*$^{Orl\ +/+}$ mice did not change significantly from day 1 to day 25 (Fig. 1c). The metastatic spread of 4T1 cells to the lungs was assessed by a micrometastasis assay. In *rl*$^{Orl\ +/+}$ mice, the tumor cells on average comprised 0.36% of all cells in lung suspensions (Fig. 1d). We observed a significant reduction of the metastatic burden in the lungs of *rl*$^{Orl\ -/-}$ mice (Fig. 1d, e).

To determine if the decrease in lung metastasis in *rl*$^{Orl\ -/-}$ mice was correlated with the size of the primary tumor, metastatic burden was compared in mice bearing similar-sized tumors. For these studies, we allowed tumor growth to progress in some *rl*$^{Orl\ -/-}$ mice until the tumors reached the equivalent size as those seen in wild type controls at 25 days after 4T1 implantation. Lung tissue samples were collected from *rl*$^{Orl\ -/-}$ mice at 29 days after 4T1 injections and used for micrometastasis assays. Metastatic burden in these animals was not significantly different from wild type controls ($p = 0.48$), suggesting that metastatic capacity of 4T1 cells was not impeded, but that metastatic progression was correlated with tumor size

(Additional Files: Fig. S1a, b). These results suggest that the absence of reelin from the host environment impedes growth of primary 4T1-derived tumors *in vivo*.

Reelin does not directly affect migration or growth of 4T1 cells *in vitro*

Next, we asked whether reelin could impact tumor growth via direct effects on 4T1 cells. Previous studies showed that primary mammary epithelial cells (MECs) normally express reelin, Dab1, and the reelin receptors ApoER2 and VLDLR [13]. We assessed the expression of the reelin pathway components in 4T1 cells by qPCR, and found that both *reelin* and *Dab1* were significantly downregulated in comparison to normal MECs (Fig. 2a). 4T1 cells expressed higher levels of *ApoER2*, while expression levels of *Vldlr* were similar to those in primary MECs (Fig. 2a). Primary MECs respond to reelin by slowing their migration rate [13], and we hypothesized that this effect would be abolished in 4T1 cells because they lacked Dab1. As we expected, 4T1 cells did not respond to reelin in the conditioned medium from reelin-expressing HEK293T cells in transwell assays (Fig. 2b). The proliferation of 4T1 cells was also unaltered in the presence of reelin (Fig. 2c). Full-length reelin (400 kD), as well as two smaller reelin fragments (300 kD, 180 kD) resulting from protein processing were all present in the conditioned medium from reelin-expressing HEK293T cells (Fig. 2d), suggesting that these results were not due to lack of available reelin. Thus, despite the expression of canonical reelin receptors in 4T1 cells, reelin does not appear to directly modulate the growth or migration of 4T1 cells *in vitro*.

Primary tumors grown in $rl^{Orl\ -/-}$ mice display alterations in blood vessel formation

Histological analysis of the primary tumors from $rl^{Orl\ -/-}$ mice did not reveal gross morphological differences from $rl^{Orl\ +/+}$ controls. In both cohorts, layers of tumor cells and infiltrating immune cells surrounded the necrotic tumor core (Fig. 3a, b). Cell proliferation, as assessed by Ki67 staining, was also not significantly different in $rl^{Orl\ -/-}$ animals (Fig. 3c, d). Tumor angiogenesis was impeded, as significantly fewer CD31-positive blood vessels were observed in primary tumors from $rl^{Orl\ -/-}$ mice (Fig. 3e, f). However, analysis of angiogenic gene expression in primary tumors by qPCR showed no differences in levels of vascular endothelial growth factors A, B, and C (*Vegfa*, *Vegfb*, *Vegfc*), or transforming growth factor β (*Tgfb*) (Fig. 4). Additionally, levels of the anti-angiogenic factor chemokine (C-X-C motif) ligand 10 (*Cxcl10*) were not significantly different (Fig. 4).

TAMs are altered in the absence of reelin

Progression of 4T1 tumors is marked by the expansion of the myeloid cell compartment, with subsequent infiltration by immune cells, such as tumor associated macrophages (TAMs), into the primary tumor microenvironment [27]. TAMs are recognized as major contributors to tumor angiogenesis [28]. Mice with the *reeler* mutation were previously reported to have deficits in the function of macrophages and T cells [29]. We hypothesized that the $rl^{Orl\ -/-}$ environment may lead to alterations in the number or function of TAMs, which could contribute to the reduction in tumor angiogenesis. Consistent with this hypothesis, we saw increased levels of the chemokine *Cxcl5* and the matrix metalloproteinase 9 (*Mmp-9*) mRNA in tumors from $rl^{Orl\ -/-}$ mice (Fig. 4). CXCL5 and MMP-9 are factors secreted by TAMs and other myeloid cells [30], and we reasoned that their augmented expression may be indicative of elevated numbers of TAMs in the primary

tumors from *rl*$^{Orl\ -/-}$ animals. Labeling of primary tumor sections with α-F4/80 antibody, a marker of TAMs [27], showed an increase in the area occupied by F4/80-positive cells in tumors from *rl*$^{Orl\ -/-}$ mice (Fig. 5a, b, c). Thus, the elevated levels of CXCL5 and MMP-9 in the tumors from mice that lack reelin may be due to an increase in TAM infiltration.

The activation state of TAMs determines their effect on cancer progression. M2-activated macrophages promote tumor angiogenesis and provide a variety of factors to elicit a sustained tumor-promoting Type 2 immune response. In contrast, abundance of M1-activated TAMs impedes angiogenesis and tumor growth, and results in a tumoricidal Type 1 immune response [31, 32]. To test whether reelin influenced the M1/M2 balance in TAMs, we examined the expression levels of several cytokines associated with M1 and M2 macrophages in the primary tumors from *rl*$^{Orl\ -/-}$ mice and wild type controls (Fig. 5d). Absence of reelin from the host environment resulted in altered levels of these genes. Specifically, we observed increased levels of a hallmark M1 cytokine inducible nitric oxide synthase (*iNOS*), while the levels of arginase 1 (*Arg1*) and mannose receptor, C Type 1 (*Mrc1*) mRNA, two genes expressed by M2-activated macrophages [31, 33], were downregulated in primary tumors from *rl*$^{Orl\ -/-}$ mice (Fig. 5d). Western blotting confirmed the reduction in Arg1 levels (Fig. 5e, f). Additionally, we observed higher levels of interleukin-10 (*IL-10*) in tumors from *rl*$^{Orl\ -/-}$ mice (Fig. 5d). IL-10 is a broadly expressed cytokine with anti-inflammatory properties, and is produced in response to factors that promote a Type 1 immune response [34, 35].

To assess the effect of 4T1 cells on *rl*$^{Orl\ -/-}$ macrophages, we cultured bone marrow-derived macrophages from *rl*$^{Orl\ -/-}$ mice and wild type controls in the presence of 4T1-conditioned medium (Additional Files: Fig. S2). Similar to observations in primary tumors, levels of *iNOS* were slightly increased in *rl*$^{Orl\ -/-}$ macrophages treated with 4T1-conditioned medium, while levels of *Arg1* and *Mrc1* were slightly decreased. However, *IL-10* levels were not significantly different in *rl*$^{Orl\ -/-}$ macrophages treated with 4T1-conditioned medium than in wild type control macrophages. Our results indicate that in the absence of reelin, TAMs may shift to an M1-like state and elicit a tumor-restrictive Type 1 immune response.

Absence of reelin skews the M1 activation state of bone marrow-derived macrophages

To test if macrophage activation was altered in the absence of reelin, we differentiated bone marrow-derived macrophages (BMDM) from *rl*$^{Orl\ -/-}$ mice and wild type controls and polarized them to an M1 state with interferon-γ (IFNγ) and lipopolysaccharide (LPS) [36]. IFNγ and LPS treatment robustly induced the expression of M1-associated genes *IL-1β, IL-6, IL-12*, tumor necrosis factor-a (*Tnfa*), and *iNOS* (Additional Files: Fig. S3). Unstimulated *rl*$^{Orl\ -/-}$ BMDM expressed higher levels of *IL-1β* compared to unstimulated wild type control BMDM, while the expression of other M1 genes was not altered (Fig. 6a). M1-polarized *rl*$^{Orl\ -/-}$ macrophages expressed significantly higher levels of *IL-6* and *iNOS* compared to wild type control M1 macrophages (Fig. 6b). In addition, levels of *IL-10* were 3-fold higher in M1 macrophages from *rl*$^{Orl\ -/-}$ mice compared to control M1 macrophages. In this model of M1 macrophage activation, IFNγ primes the macrophages for a rapid response to LPS, which triggers toll-like receptor (TLR) signaling and production of

cytokines associated with the Type 1 immune response [37]. TLR signaling induces IL-10 expression in macrophages in order to negatively regulate the inflammatory response [34, 38, 39]. Our results suggest that the upregulation of IL-10 in *rl*$^{Orl\ -/-}$ mice may be a part of a similar negative feedback mechanism. Thus, BMDM display a higher propensity towards M1 activation in the absence of reelin.

Discussion

The goal of the studies presented here was to better understand the role of reelin signaling in breast cancer growth and metastatic progression. We found that reelin deficiency delays primary tumor growth and lung metastasis. We showed that 4T1 cells do not lose their metastatic capacity in the absence of reelin. Previous studies reported that the size of the primary 4T1 tumor correlated with the extent of the metastatic burden [40, 41], and 4T1 cells metastasized primarily via blood vessels [42]. In agreement with these results, we found that the reduction in lung metastases in *rl*$^{Orl\ -/-}$ mice is likely due to the smaller size and poor vascularization of the primary tumors.

Although reelin did not directly affect proliferation or migration of 4T1 cells *in vitro*, we cannot rule out the possibility that reelin affects 4T1 cells via alternative mechanisms. For example, absence of reelin may lead to alterations in the gene expression profile of 4T1 cells, resulting in a tumor-restrictive microenvironment. The reduction in CD31-positive labeling of primary tumors from *rl*$^{Orl\ -/-}$ mice suggested a deficit in tumor angiogenesis. Surprisingly, we observed increased levels of the *Mmp-9* transcript in primary tumors from *rl*$^{Orl\ -/-}$ mice. MMP-9 activity is provided by myeloid cells in the tumor microenvironment and is required for tumor vasculogenesis [43]. However, the pro-angiogenic effects of MMP-9 are contingent on its activation via a proteolytic cascade [43]. The absence of reelin could affect the activation of MMP-9, but we cannot make definitive conclusions based on the available data. Alternatively, the deficit in vascularization of tumors in the absence of reelin could be due to alterations in endothelial cells, but past studies did not find a role for reelin in angiogenesis, and the vascular network of *reeler* mice is normal [12, 44, 45].

The increased levels of M1-specific iNOS and decreased levels of M2-specific Arg1 in primary tumors from *rl*$^{Orl\ -/-}$ mice indicate the predominance of M1-activated TAMs that may impede tumor growth and angiogenesis. In addition, macrophages from *rl*$^{Orl\ -/-}$ mice display increased propensity for M1 activation. These results suggest that reelin may affect activation of macrophages in the tumor microenvironment. The influence of reelin signaling on the development and function of the immune system has not been studied extensively. However, one study found functional deficits in macrophages and T cells from *reeler* $^{-/-}$ animals on a C57/B6 background [29]. These *reeler* mutants differ from our model because they completely lack reelin. In addition, peritoneal macrophages from these mice showed elevated production of IL1β when activated by LPS *in vitro* [46, 47]. Another group proposed a role for reelin in clustering of the serotonin transporter (SERT) in blood lymphocytes, as peripheral lymphocytes from *reeler* $^{-/-}$ mice displayed spreading of the SERT clusters [48]. However, we cannot rule out the possibility that other cell types in the tumor microenvironment, such as stromal fibroblasts, myeloid-derived suppressor cells or

tumor-infiltrating lymphocytes, may also be affected by the loss of host-derived reelin, causing a delay in tumor progression. These possibilities can be addressed in future studies.

Previous studies on reelin signaling in the context of tumor progression focused mainly on the expression of reelin pathway components in the primary tumor tissue, or in cancer cell lines [14,18, 49–51]. For instance, downregulation of reelin was observed in primary breast tumors, and loss of reelin expression correlated with poor survival. In addition, reelin expression was epigenetically silenced in breast cancer cell lines [18]. It is therefore interesting that in our model, loss of functional reelin protein in the host environment delayed the growth of normally aggressive 4T1 tumors. However, our finding that the 4T1 cell line does not express reelin correlates with previously published results. The human triple-negative breast cancer cell line MDA-MB-231 was reported to have a low baseline expression of reelin [18]. Transfection of this cell line with the full-length reelin construct decreased the migratory and invasive potential of MDA-MB-231 cells [18]. Because reelin impedes the migration of epithelial cells, the results of previous studies imply that cancer cells may downregulate reelin expression in order to become more migratory and invasive. On the other hand, our studies demonstrate that reelin may be necessary for tumor-promoting responses of host immune cells, and therefore may play a dual role in cancer progression.

In summary, our findings provide evidence for additional non-neuronal functions of reelin. Our data demonstrate that absence of host-derived reelin delays mammary tumor growth and metastatic progression. Our observations offer insight into the importance of stromal reelin in breast cancer progression, and suggest a potential role for reelin in the development and function of the innate immune system.

Supplementary Material

Refer to Web version on PubMed Central for supplementary material.

Acknowledgments

We thank Dr. Patricia Phelps, Dr. Cristina Ghiani, Dr. Catalina Abad Rabat and Dr. Diana Moughon for kindly providing reagents and for thoughtful discussion. We are thankful to Donna Crandall for assistance with figure preparation and Joseph Argus for assistance with manuscript editing.

Grants

These studies were supported by the National Institute of Child Health and Development R03 HD075840 - https://www.nichd.nih.gov/Pages/index.aspx and the California Breast Cancer Research Program 161B-0110 - http://www.cbcrp.org/ to EMC. EK was supported by the Whitcome Fellowship of the UCLA Molecular Biology Institute. The funders had no role in study design, data collection and analysis, decision to publish, or preparation of the manuscript.

References

1. Fatemi, SH. Reelin glycoprotein: structure, biology, and roles in health and disease. New York, NY: Springer; 2008.
2. Honda T, Kobayashi K, Mikoshiba K, Nakajima K. Regulation of cortical neuron migration by the reelin signaling pathway. Neurochem Res. 2011; 36(7):1270–1279. [PubMed: 21253854]

3. Abadesco AD, Cilluffo M, Yvone GM, Carpenter EM, Howell BW, Phelps PE. Novel Disabled-1-expressing neurons identified in adult brain and spinal cord. Eur J Neurosci. 2014; 39:579–592. [PubMed: 24251407]
4. D'Arcangelo G. Reelin in the years: controlling neuronal migration and maturation in the mammalian brain. Adv Neurosci. 2014 Article ID 597395.
5. Herz J, Chen Y. Reelin, lipoprotein receptors and synaptic plasticity. Nat Rev Neurosci. 2006; 7(11): 850–859. [PubMed: 17053810]
6. Bock HH, Herz J. Reelin activates SRC family tyrosine kinases in neurons. Curr Biol. 2003; 13(1): 18–26. [PubMed: 12526740]
7. Kuo G, Arnaud L, Kronstad-O'Brien P, Cooper JA. Absence of Fyn and Src causes a reeler-like phenotype. J Neurosci. 2005; 25(37):8578–8586. [PubMed: 16162939]
8. Diaz-Mendoza MJ, Lorda-Diez CI, Montero JA, Garcia-Porrero JA, Hurle JM. Reelin/DAB-1 signaling in the embryonic limb regulates the chondrogenic differentiation of digit mesodermal progenitors. J Cell Physiol. 2014; 229(10):1397–1404. [PubMed: 24519818]
9. Botella-López A, de Madaria E, Jover R, Bataller R, Sancho-Bru P, Candela A, et al. Reelin is overexpressed in the liver and plasma of bile duct ligated rats and its levels and glycosylation are altered in plasma of humans with cirrhosis. Int J Biochem Cell Biol. 2008; 40(4):766–775. [PubMed: 18449964]
10. Tseng WL, Chen TH, Huang CC, Huang YH, Yeh CF, Tsai HJ, et al. Impaired thrombin generation in Reelin-deficient mice: a potential role of plasma Reelin in hemostasis. J Thromb Haemost. 2014; 12(12):1–11. [PubMed: 24916373]
11. Vázquez-Carretero MD, García-Miranda P, Calonge ML, Peral MJ, Ilundain AA. Dab1 and reelin participate in a common signal pathway that controls intestinal crypt/villus unit dynamics. Biol Cell. 2014; 106(3):83–96. [PubMed: 24313315]
12. Lutter S, Xie S, Tatin F, Makinen T. Smooth muscle-endothelial cell communication activates Reelin signaling and regulates lymphatic vessel formation. J Cell Biol. 2012; 197(6):837–849. [PubMed: 22665518]
13. Khialeeva E, Lane TF, Carpenter EM. Disruption of reelin signaling alters mammary gland morphogenesis. Development. 2011; 138(4):767–776. [PubMed: 21266412]
14. Hong SM, Kelly D, Griffith M, Omura N, Li A, Li CP, et al. Multiple genes are hypermethylated in intraductal papillary mucinous neoplasms of the pancreas. Mod Pathol. 2008; 21(12):1499–1507. [PubMed: 18820670]
15. Dohi O, Takada H, Wakabayashi N, Yasui K, Sakakura C, Mitsufuji S, et al. Epigenetic silencing of RELN in gastric cancer. Int J Oncol. 2010; 36(1):85–92. [PubMed: 19956836]
16. Perrone G, Vincenzi B, Zagami M, Santini D, Panteri R, Flammia G, et al. Reelin expression in human prostate cancer: a marker of tumor aggressiveness based on correlation with grade. Mod Pathol. 2007; 20(3):344–351. [PubMed: 17277764]
17. Wang Q, Lu J, Yang C, Wang X, Cheng L, Hu G, et al. CASK and its target gene Reelin were co-upregulated in human esophageal carcinoma. Cancer Lett. 2002; 179(1):71–77. [PubMed: 11880184]
18. Stein T, Cosimo E, Yu X, Smith PR, Simon R, Cottrell L, et al. Loss of reelin expression in breast cancer is epigenetically controlled and associated with poor prognosis. Am J Pathol. 2010; 177(5): 2323–2333. [PubMed: 20847288]
19. Pulaski BA, Ostrand-Rosenberg S. Mouse 4T1 breast tumor model. Curr Protoc Immunol. 2001 Chapter 20:Unit 20.2.
20. Takahara T, Ohsumi T, Kuromitsu J, Shibata K, Sasaki N, Okazaki Y, et al. Dysfunction of the Orleans reeler gene arising from exon skipping due to transposition of a full-length copy of an active L1 sequence into the skipped exon. Hum Mol Genet. 1996; 5(7):989–993. [PubMed: 8817336]
21. De Bergeyck V, Nakajima K, Lambert de Rouvrait C, Naerhuyzen B, Goffinet AM, Miyata T, et al. A truncated Reelin protein is produced but not secreted in the "Orleans" reeler mutation (Reln(rl-Orl)). Brain Res Mol Brain Res. 1997; 50(1–2):85–90. [PubMed: 9406921]
22. D'Arcangelo G, Homayouni R, Keshvara L, Rice DS, Sheldon M, Curran T. Reelin is a ligand for lipoprotein receptors. Neuron. 1999; 24(2):471–479. [PubMed: 10571240]

23. Ewald AJ. Isolation of mouse mammary organoids for long-term time-lapse imaging. Cold Spring Harb Protoc. 2013; 2013(2):130–133. [PubMed: 23378653]
24. Kim EJ, Choi MR, Park H, Kim M, Hong JE, Lee JY, et al. Dietary fat increases solid tumor growth and metastasis of 4T1 murine mammary carcinoma cells and mortality in obesity-resistant BALB/c mice. Breast Cancer Res. 2011; 13(4):R78. [PubMed: 21834963]
25. York AG, Williams KJ, Argus JP, Zhou QD, Brar G, Vergnes L, et al. Limiting cholesterol biosynthetic flux spontaneously engages Type I IFN signaling. Cell. 2015; 163(7):1716–1729. [PubMed: 26686653]
26. Falconer D. Two new mutants, 'trembler'and 'reeler', with neurological actions in the house mouse (Mus musculus L.). J Genet. 1951; 50(2):192–205. [PubMed: 24539699]
27. DuPré SA, Redelman D, Hunter KW. The mouse mammary carcinoma 4T1: characterization of the cellular landscape of primary tumours and metastatic tumour foci. Int J Exp Pathol. 2007; 88(5): 351–360. [PubMed: 17877537]
28. Cho HJ, Jung JI, Lim DY, Kwon GT, Her S, Park JH, et al. Bone marrow-derived, alternatively-activated macrophages enhance solid tumor growth and lung metastasis of mammary carcinoma cells in a Balb/C mouse orthotopic model. Breast Cancer Res. 2012; 14(3):R81. [PubMed: 22616919]
29. Green-Johnson JM, Zalcman S, Vriend CY, Nance DM, Greenberg AH. Suppressed T cell and macrophage function in the" reeler"(rl/rl) mutant, a murine strain with elevated cerebellar norepinephrine concentration. Brain Behav Immun. 1995; 9(1):47–60. [PubMed: 7620210]
30. Murdoch C, Muthana M, Coffelt SB, Lewis CE. The role of myeloid cells in the promotion of tumour angiogenesis. Nat Rev Cancer. 2008; 8(8):618–631. [PubMed: 18633355]
31. Mills CD. M1 and M2 macrophages: oracles of health and disease. Crit Rev Immunol. 2012; 32(6): 463–488. [PubMed: 23428224]
32. Ma J, Liu L, Che G, Yu N, Dai F, You Z. The M1 form of tumor-associated macrophages in non-small cell lung cancer is positively associated with survival time. BMC Cancer. 2010; 10:112. [PubMed: 20338029]
33. Mantovani A, Sozzani S, Locati M, Allavena P, Sica A. Macrophage polarization: tumor-associated macrophages as a paradigm for polarized M2 mononuclear phagocytes. Trends Immunol. 2002; 23(11):549–555. [PubMed: 12401408]
34. Saraiva M, O'Garra A. The regulation of IL-10 production by immune cells. Nat Rev Immunol. 2010; 10(3):170–181. [PubMed: 20154735]
35. Trinchieri G. Interleukin-10 production by effector T cells: Th1 cells show self control. J Exp Med. 2007; 204(2):239–243. [PubMed: 17296790]
36. Pineda-Torra I, Gage M, de Juan A, Pello OM. Isolation, culture and polarization of murine bone marrow-derived and peritoneal macrophages. Methods Mol Biol. 2015; 1339:101–109. [PubMed: 26445783]
37. Schroder K, Hertzog PJ, Ravasi T, Hume DA. Interferon-gamma: an overview of signals , mechanisms and functions. J Leukoc Biol. 2004; 75(2):163–189. [PubMed: 14525967]
38. Boonstra A, Rajsbaum R, Holman M, Marques R, Asselin-Paturel C, Pereira JP, et al. Macrophages and myeloid dendritic cells, but not plasmacytoid dendritic cells, produce IL-10 in response to MyD88- and TRIF-dependent TLR signals, and TLR-independent signals. J Immunol. 2006; 177(11):7551–7558. [PubMed: 17114424]
39. Martinez FO, Gordon S. The M1 and M2 paradigm of macrophage activation : time for reassessment. F1000Prime Rep. 2014; 3:1–13.
40. Pulaski BA, Ostrand-Rosenberg S. Reduction of established spontaneous mammary carcinoma metastases following immunotherapy with major histocompatibility complex class II and B7.1 cell-based tumor vaccines. Cancer Res. 1998; 58(7):1486–1493. [PubMed: 9537252]
41. Thomas DL, Fraser NW. HSV-1 therapy of primary tumors reduces the number of metastases in an immune-competent model of metastatic breast cancer. Mol Ther. 2003; 8(4):543–551. [PubMed: 14529826]
42. Aslakson CJ, Miller FR. Selective events in the metastatic process defined by analysis of the sequential dissemination of subpopulations of a mouse mammary tumor. Cancer Res. 1992; 52(6): 1399–1405. [PubMed: 1540948]

43. Kessenbrock K, Plaks V, Werb Z. Matrix metalloproteinases: regulators of the tumor microenvironment. Cell. 2010; 141(1):52–67. [PubMed: 20371345]
44. Stubbs D, DeProto J, Nie K, Englund C, Mahmud I, Hevner R, et al. Neurovascular congruence during cerebral cortical development. Cereb Cortex. 2009; 19(suppl 1):32–41.
45. Guy J, Wagener RJ, Möck M, Staiger JF. Persistence of functional sensory maps in the absence of cortical layers in the somsatosensory cortex of reeler mice. Cereb Cortex. 2015; 25(9):2517–2528. [PubMed: 24759695]
46. Kopmels B, Wollman EE, Guastavino JM, Delhaye-Bouchaud N, Fradelizi D, Mariani J. Interleukin-1 hyperproduction by in vitro activated peripheral macrophages from cerebellar mutant mice. J Neurochem. 1990; 55(6):1980–1985. [PubMed: 2230805]
47. Bakalian A, Kopmels B, Messer A, Fradelizi D, Delhaye-Bouchaud N, Wollman E, et al. Peripheral macrophage abnormalities in mutant mice with spinocerebellar degeneration. Res Immunol. 1992; 143(1):129–139. [PubMed: 1565842]
48. Rivera-Baltanas T, Romay-Tallon R, Dopeso-Reyes IG, Caruncho HJ. Serotonin transporter clustering in blood lymphocytes of reeler mice. Cardiovasc Psychiatry Neurol. 2010; 2010:396282. [PubMed: 20414372]
49. Resende C, Ristimäki A, Machado JC. Genetic and epigenetic alteration in gastric carcinogenesis. Helicobacter. 2010; 15(suppl I):34–39. [PubMed: 21054651]
50. Berthier-Vergnes O, Kharbili M El, de la Fouchardière A, Pointecouteau T, Verrando P, Wierinckx A, et al. Gene expression profiles of human melanoma cells with different invasive potential reveal TSPAN8 as a novel mediator of invasion. Br J Cancer. 2011; 104(1):155–165. [PubMed: 21081927]
51. Zhang J, Ding L, Holmfeldt L, Wu G, Heatley SL, Payne-Turner D, et al. The genetic basis of early T-cell precursor acute lymphoblastic leukaemia. Nature. 2012; 481(7380):157–163. [PubMed: 22237106]

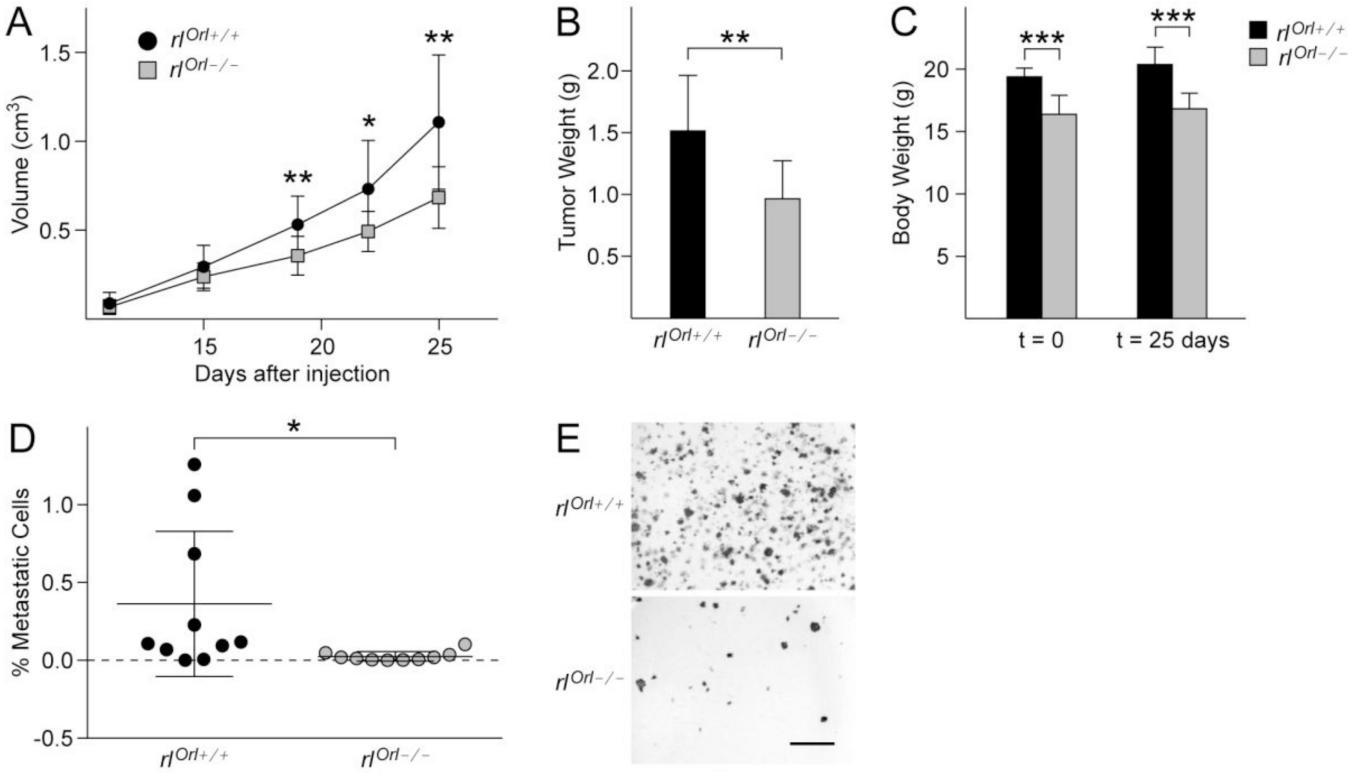

Fig. 1. 4T1 mammary tumor growth and lung metastasis in *rl*$^{Orl\ -/-}$ mice

(a) Growth of primary tumors in *rl*$^{Orl\ -/-}$ (n=10) and *rl*$^{Orl\ +/+}$ (n=10) control mice. (b) Wet weight of primary tumors collected 25 days after 4T1 cell injection. (c) Total body weight of animals on the day of 4T1 injections (t = 0) and the day of sacrifice (t = 25 days). (d) Quantification of metastatic burden in the lungs. (e) Representative images of 4T1-derived metastatic colonies from the lungs of *rl*$^{Orl\ +/+}$ and *rl*$^{Orl\ -/-}$ mice used for quantification in (d). Bar = 5 mm. *P < 0.05, **P < 0.01, ***P < 0.001. Statistical significance determined using two-tailed, unpaired Student's t-test.

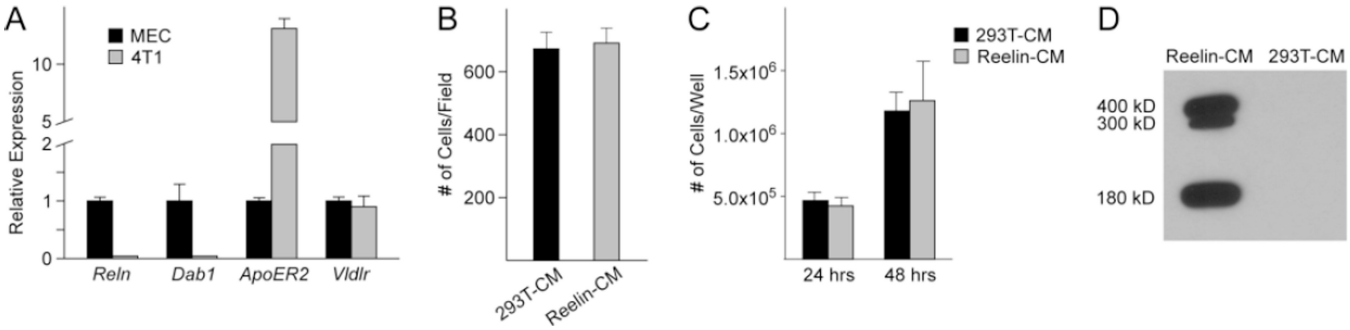

Fig. 2. Expression of reelin signaling pathway components and the effect of reelin on growth and migration of 4T1 cells

(a) qPCR analysis of relative expression levels of reelin signaling pathway components in 4T1 cells. Gene expression levels are normalized to those in wild type mammary epithelial cells (MEC). (b) Transwell migration assay of 4T1 cells in the presence of reelin conditioned media (Reelin-CM) or controlled conditioned media (293T–CM). (c) Number of 4T1 cells grown in the presence or absence of reelin for 24 or 48 hours. (d) Western blot of reelin expression in conditioned media from reelin expressing HEK293T cells (Reelin-CM) or conditioned media from control cells (293-CM). 20 μg of total protein were loaded into each lane.

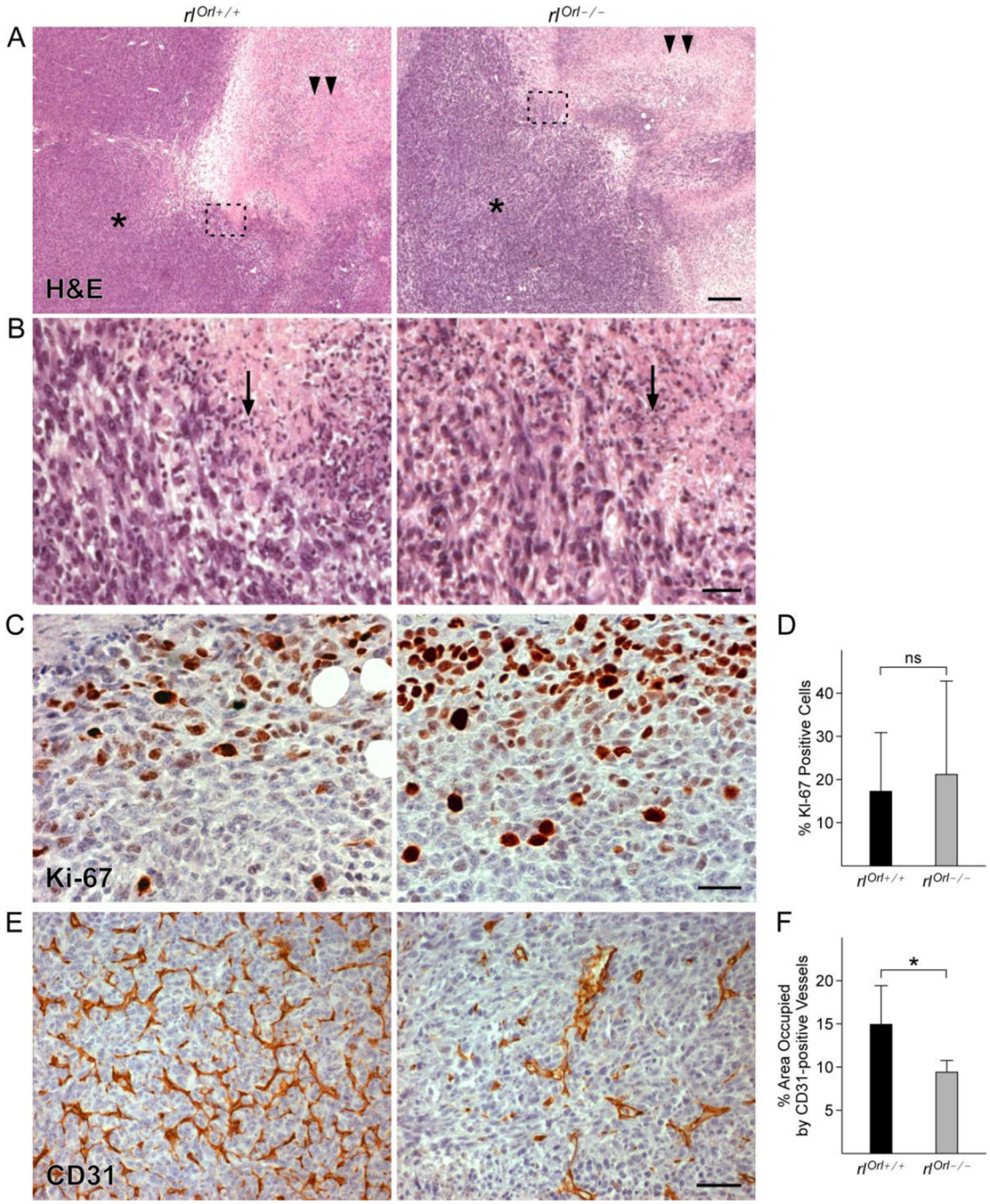

Fig. 3. Characterization of proliferation and angiogenesis in primary tumors from *rl*$^{Orl/}$ mice

(a) H&E staining of primary tumors from *rl*$^{Orl\ -/-}$ and *rl*$^{Orl\ +/+}$ control mice. Asterisk - tumor cells, double arrowheads – necrotic core. Bar = 200 μm. (b) High magnification view of the areas outlined in (A). Arrow - infiltrating immune cells. Bar = 30 μm. (c) Ki-67 labeling of primary tumors from *rl*$^{Orl\ -/-}$ and *rl*$^{Orl\ +/+}$ mice. Bar = 30 μm. (d) Quantification of (c), *rl*$^{Orl\ +/+}$ n=7, *rl*$^{Orl\ -/-}$: n=7. (e) CD31 labeling of primary tumors from *rl*$^{Orl\ -/-}$ and *rl*$^{Orl\ +/+}$mice. Bar = 50 μm. (f) Quantification of (e), *rl*$^{Orl\ +/+}$ n=7, *rl*$^{Orl\ -/-}$: n=6. ns - not

significant, *P < 0.05. Statistical significance determined using two-tailed, unpaired Student's t-test.

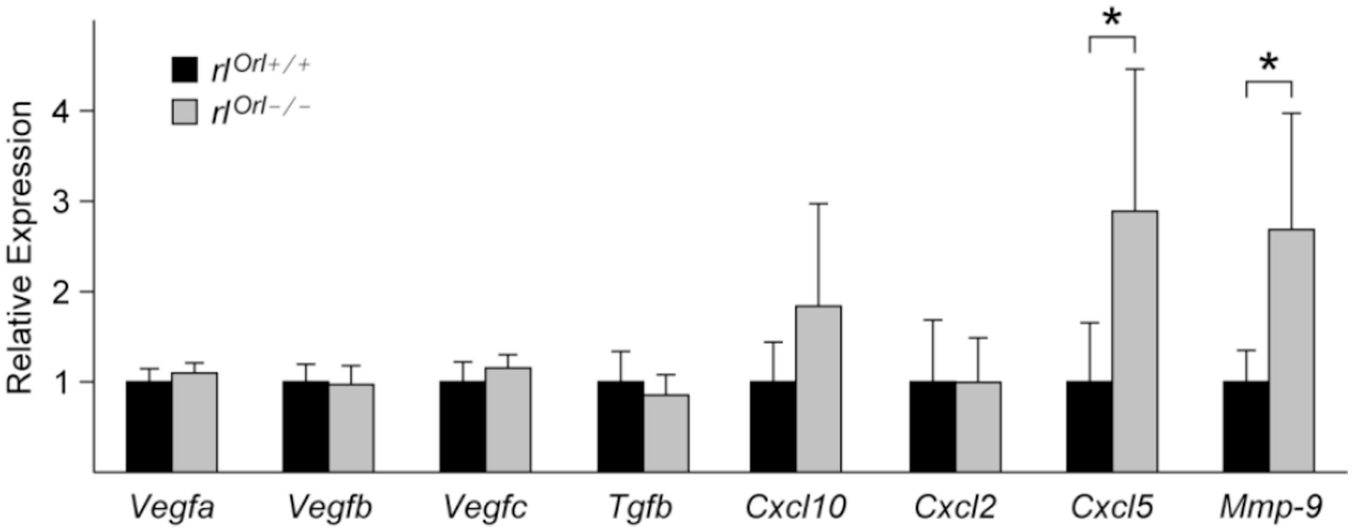

Fig. 4. Gene expression analysis of primary tumors from *rl*$^{Orl\ -/-}$ mice

qPCR analysis of angiogenic genes (*Vegfa, Vegfb, Vegfc, Tgfb*), chemokines (*Cxcl10, Cxcl2, Cxcl5*), and metalloproteinase *Mmp-9* in primary tumors from *rl*$^{Orl\ -/-}$ mice. Gene expression levels are relative to those in tumors from *rl*$^{Orl\ +/+}$ controls. *P < 0.05. Statistical significance determined using two-tailed, unpaired Student's t-test.

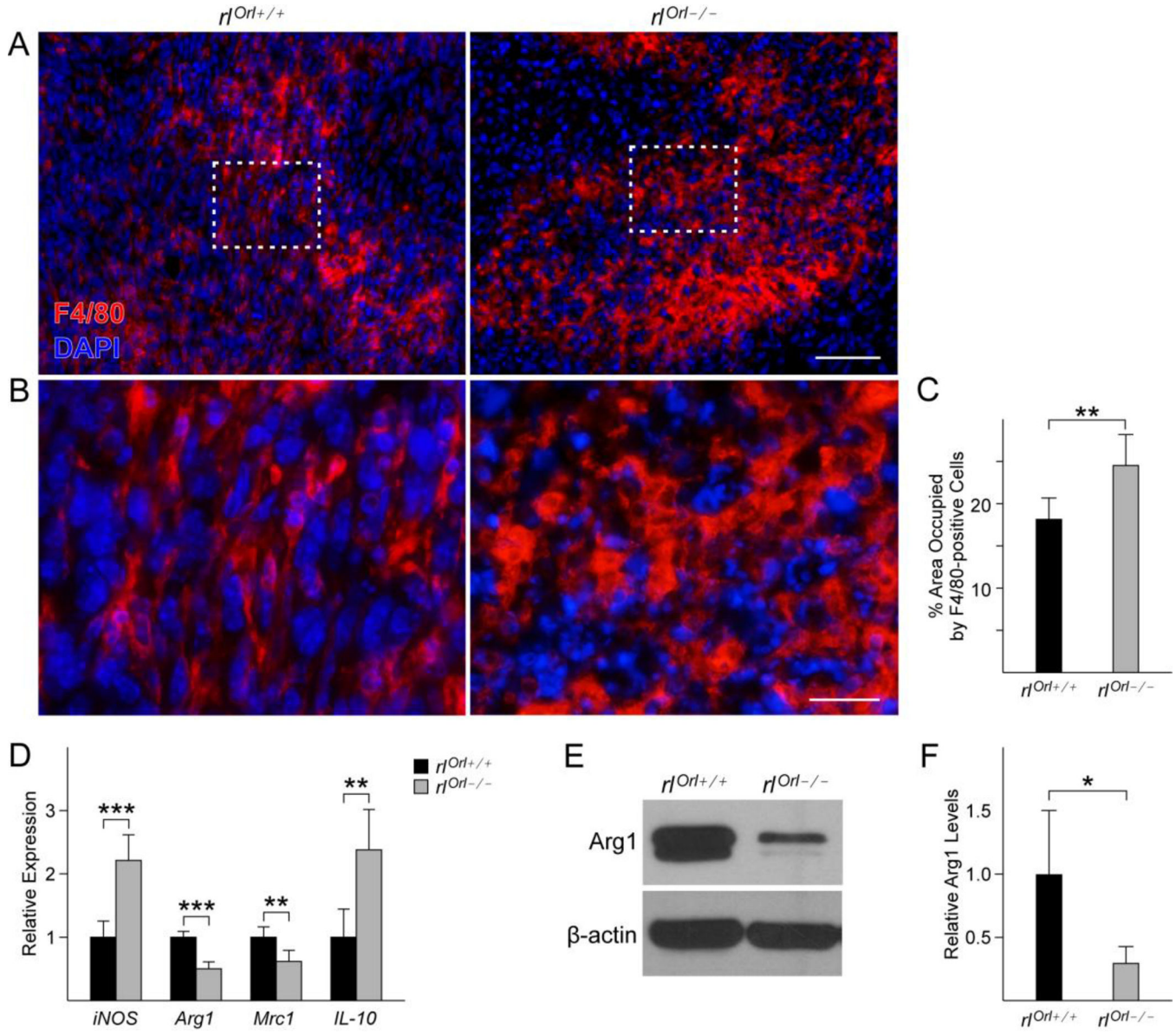

Fig. 5. Analysis of tumor associated macrophages in primary tumors from *rl*$^{Orl\ -/-}$ mice

(a) F4/80 labeling of primary tumors from *rl*$^{Orl\ -/-}$ and *rl*$^{Orl\ +/+}$ mice. Bar = 50 μm. (b) High magnification view of the areas outlined in (a). Bar = 20 μm. (c) Quantification of the area occupied by F4/80-positive cells, *rl*$^{Orl\ +/+}$ n=6, *rl*$^{Orl\ -/-}$: n=6. (d) qPCR analysis of *iNOS* (M1), *Arg1* (M2), *Mrc1 (M2)*, and *IL-10* gene expression in primary tumors from *rl*$^{Orl\ -/-}$mice, gene expression levels are relative to those in tumors from *rl*$^{Orl\ +/+}$ controls. (e) Western blot of Arg1 and β-actin expression in primary tumors from *rl*$^{Orl\ -/-}$ and *rl*$^{Orl\ +/+}$mice. (f) Quantification of band intensities in (e). *P < 0.05, **P < 0.01, ***P < 0.001. Statistical significance determined using two-tailed, unpaired Student's t-test.

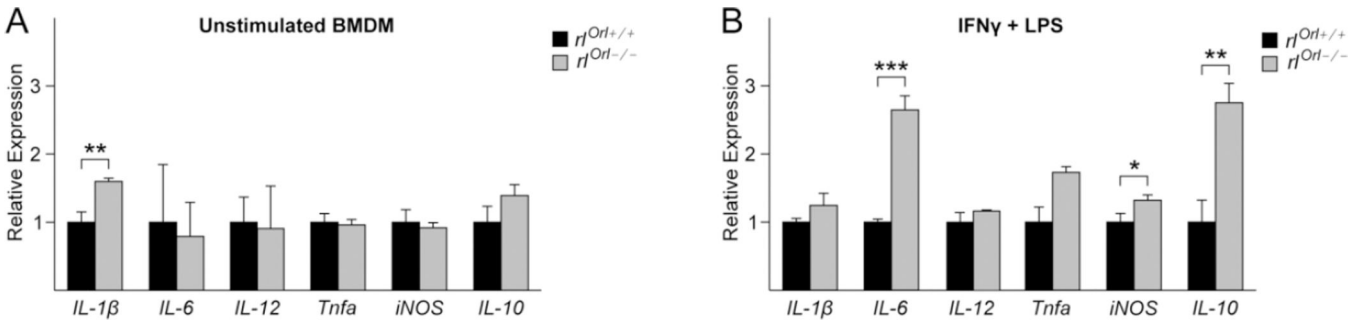

Fig. 6. Cytokine expression levels in baseline and M1-polarized BMDM from *rl*$^{Orl\ -/-}$ mice

(a, b) *IL-1β* (M1), *IL-6* (M1), *IL-12* (M1), *Tnfa* (M1), *iNOS* (M1), and *IL-10* mRNA expression levels in (a) unstimulated BMDM and (b) M1-polarized BMDM from *rl*$^{Orl\ -/-}$mice, analyzed by qPCR. Gene expression levels are relative to those in the respective *rl*$^{Orl\ +/+}$ BMDM controls. *P < 0.05, **P < 0.01, ***P < 0.001. Statistical significance determined using two-tailed, unpaired Student's t-test.

Table 1

Primers used for qPCR gene expression analysis.

Gene	Forward Primer (5' - 3')	Reverse Primer (5' - 3')
ApoER2	CGGACAGCGACTTCACCT	CTTCTCGGCAGGACACTCTT
Arg1	GCAGAGGTCCAGAAGAATGG	AGCATCCACCCAAATGACAC
Cxcl2	AATCATCCAAAAGATACTGAACAAAG	TTCTCTTTGGTTCTTCCGTTG
Cxcl5	TGCGTTGTGTTTGCTTAACCG	CTTCCACCGTAGGGCACTG
Cxcl10	CCAAGTGCTGCCGTCATTTTC	GGCTCGCAGGGATGATTTCAA
Dab1	GATGAAGTGTCCGCAGCTC	GTGTTCTCCCTTGGAACGTG
IL-1b	GCCCATCCTCTGTGACTCAT	AGGCCACAGGTATTTTGTCG
IL-6	AGTTGCCTTCTTGGGACTGA	TCCACGATTTCCCAGAGAAC
IL-10	GCTCTTACTGACTGGCATGAG	CGCAGCTCTAGGAGCATGTG
IL-12	CCATCAGCAGATCATTCTAGACAA	CGCCATTATGATTCAGAGACTG
iNOS	CACCTTGGAGTTCACCCAGT	ACCACTCGTACTTGGGATGC
Mmp-9	GGACCCGAAGCGGACATTG	CGTCGTCGAAATGGGCATCT
Mrc1	ATTGTGGAGCAGATGGAAGG	TGAATGGAAATGCACAGACG
Reln	GTCACGGTCTACCTGCCACT	TCAATAGCCCAGGAATCTGC
Tgfb	TTGCTTCAGCTCCACAGAGA	TGGTTGTAGAGGGCAAGGAC
Tnfa	TGCCTATGTCTCAGCCTCTTC	GAGGCCATTTGGGAACTTCT
Vegfa	GGAGAGCAGAAGTCCCATGA	GGGGTACTCCTGGAAGATGTC
Vegfb	TCTGAGCATGGAACTCATGG	TCTGCATTCACATTGGCTGT
Vegfc	CAAGGCTTTTGAAGGCAAAG	TGCTGAGGTAACCTGTGCTG
Vldlr	TACCCTAGACGGAGCCAAGA	GTAAACAAAGCCCGACAACG